

## Wind tunnel tests on flow fields of full-scale railway wind barriers

Yang Su<sup>a</sup>, Huoyue Xiang<sup>\*</sup>, Chen Fang<sup>b</sup>, Lei Wang<sup>c</sup> and Yongle Li<sup>d</sup>

*Department of Bridge Engineering, Southwest Jiaotong University, Chengdu, Sichuan 610031, China*

*(Received June 12, 2016, Revised December 4, 2016, Accepted December 6, 2016)*

**Abstract.** The present study provides a deeper understanding of the flow fields of a full-scale railway wind barriers by means of a wind tunnel test. First, the drag forces of the three wind barriers were measured using a force sensor, and the drag force coefficients were compared with a similar scale model. On this basis, the mean wind velocity and turbulence upwind and downwind of the wind barriers were measured. The effects of pore size and opening forms of the wind barrier were discussed. The results show that the test of the scaled wind barrier model may be unsafe, and it is suitable to adopt the full-scale wind barrier model. The pore size and the opening forms of wind barriers have a slight influence on the flow fields upwind of the wind barrier but have some influences on the flow fields and power spectra downwind of the wind barrier. The smaller pore size generates a lower turbulence density and value of the power spectrum near the wind barrier, and the porous wind barriers clearly provide better shelter than the bar-type wind barriers.

**Keywords:** wind barrier; full-scale; wind tunnel test; flow fields; power spectra

---

### 1. Introduction

With the rapid development of high-speed railways, the safety of trains under crosswinds becomes increasingly more important. As one of the most important and effective measures, wind barriers are used to reduce wind-induced accidents of trains, so the study on wind barriers becomes a matter of increasing concern. Presently, three methods are applied to study the performance of wind barriers: field experiments, numerical simulation and wind tunnel testing.

The field experiment is an important method because it simulates the actual wind barriers. Early articles on the field study of windbreaks were concentrated on the agriculture field (Bofah and Al-Hinai 1986, Schwartz, Fryrear *et al.* 1995, Boldes, Colman *et al.* 2001). Field data about wind barriers used in the traffic field was rarely provided. Richardson (1995) investigated the characteristics of turbulence in the presence of porous wind barriers, and the results showed that the frequencies of the generated turbulence were related to the velocity gradients in the region where the generation occurred. Wang, Wang *et al.* (2013) studied the effect of vehicle type and vehicle speed on imperforated wind barriers, but they did not focus on the effect of crosswinds.

---

\*Corresponding author, Lecture, E-mail: [hy@swjtu.edu.cn](mailto:hy@swjtu.edu.cn)

<sup>a</sup> Ph.D. Candidate, E-mail: [pkingdream@126.com](mailto:pkingdream@126.com)

<sup>b</sup> Ph.D. Candidate, E-mail: [1454457971@qq.com](mailto:1454457971@qq.com)

<sup>c</sup> Master Student, E-mail: [wangleiyuhua@163.com](mailto:wangleiyuhua@163.com)

<sup>d</sup> Professor, E-mail: [lele@swjtu.edu.cn](mailto:lele@swjtu.edu.cn)

Field experiments on railway wind barriers are limited because of the security and difficulty of the experiment.

Regarding numerical simulation, Telenta, Duhovnik *et al.* (2014), Telenta, Batista *et al.* (2015) focused on a parametric numerical study of the wind barrier's bar inclination shelter effect in crosswind scenario. Xiang, Li *et al.* (2015b) investigated the flow characteristics of the turbulent wake behind the wind barrier and discussed the protective effects of wind barriers on moving trains by means of CFD. Chu, Chang *et al.* (2013) investigated the protective effect of porous windbreak on road vehicles against crosswind by a large eddy simulation (LES) model. A detailed parameter study, including porosity, height, and the distance between the adjacent fences, was conducted by Bitog, Lee *et al.* (2009). On the whole, the numerical simulation has some superiority over wind barriers with simple opening forms. However, the accuracy of the method remains to be further improved when the holes of wind barriers are very small and complicated.

Wind tunnel testing is another effective method to explore the characteristics of wind barriers. A series of work has been carried out by many scholars. Coleman and Baker (1992) used a 1/50th scale model to study the aerodynamic effect of wind barriers on road vehicles. Chen, Li *et al.* (2015) investigated the effects of wind barriers on the safety of vehicles driven on large bridges. Kozmar, Procino *et al.* (2012) tested the flow field characteristics in the wake of a wind barrier by PIV. Xiang, Li *et al.* (2014) measured the wind loads of a train and the wind pressure distribution above the track, and then the protection effect of a railway wind barrier on the running safety of a train under cross winds was explored. Wu, Zou *et al.* (2013) compared the protective effect of wind barriers of different porosity, row space and row number based on wind tunnel measurements and suggested the optimal porosity of 0.3–0.4 for wind barriers. Guo, Wang *et al.* (2015) investigated the aerodynamic effect of wind barriers on static vehicles by wind tunnel testing. Xiang, Li *et al.* (2015a) investigated the aerodynamic loads on wind barriers under uniform flow and discussed the effect of aerodynamic interactions between static vehicles and wind barriers. In previous studies, scale models were used to study the performance of wind barriers, but it was difficult to satisfy the geometric similarity absolutely and the Reynolds number effects were not neglected. Because of the scale effect, errors would be found in the results when the holes of wind barriers were small (Xiang 2013).

Wind tunnel tests feature lower costs and easier operation, and a full-scale wind barrier model could avoid the impact of the scale effect and simulate the local details of wind barriers accurately. Therefore, full-scale wind barrier models are developed for wind tunnel tests in our study. In Section 2, the test methodologies of the full-scale wind barrier are introduced. In Section 3, the drag forces of the full-scale wind barrier are discussed by comparison to the scaled model. On this basis, Section 4 discusses the effects of the pore size and opening forms of the full-scale wind barrier on the flow fields and power spectra upwind and downwind of wind barriers.

## 2. Test methodology of full-scale wind barriers

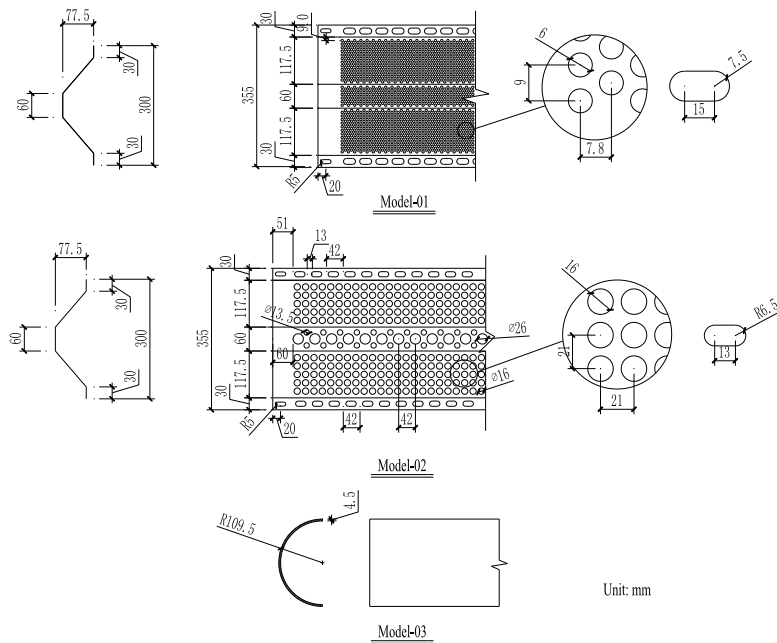
The experiments are conducted in the wind tunnel XNJD-3 with a top velocity near 16.5 m/s. The turbulence intensity of the free-stream flow  $I_x$  is less than 1.5%. It is a closed-circuit facility and comprises of a boundary test section that is 36 m long, 22.5 m wide and 4.5 m high.

The test is carried out for three cases of wind barrier strips (see Fig. 1 and Table 1), which are produced according to the requirements of engineering. Porosities of the whole wind barriers are 36.5% for model-1 and model-2 and 34.4% for model-3. The columns and cross beams are not

considered when calculating the porosities. These porosities are found to have better flow characteristics in abating particle erosion with small turbulence fluctuations and large mean velocity reduction (Lee and Kim 1999). The height and length of the whole railway wind barriers are 3.5 m and 4.4 m, respectively (see Fig. 2(a)). Model-1 and model-2 could be used to investigate the impact of the pore sizes. Model-2 and model-3 could be used to study the effect of the opening forms, although a slight difference of 2% exists between the porosities of the two barriers. All of these wind barriers are simulated in wind environments with uniform flow.



(a) The forming diagram of strip models



(b) The detailed sizes of strip models

Fig. 1 Three cases of wind barrier strips



Fig. 2 Wind barrier models in the wind tunnel

Considering the influences of the blockage ratio of the full-scale models, the wind barrier is placed perpendicularly to the wind direction and vertically placed in the wind tunnel. If a line structure such as a bridge or high embankment is considered, the blockage ratio will be unacceptable. Therefore, flat ground is used to approximately simulate the line structures. The section models of wind barriers and the detailed size of the framework are shown in Fig. 2. The illustration of the wind barrier model and the coordinate system used in the wind tunnel tests are shown in Fig. 3. We can then calculate the blockage ratio of the models (15.6%) by using the height of the wind barrier to divide the width of the tunnel. Neglecting the porous part, the blockage ratio is only 9.9%.

It is difficult to measure the forces of entire wind barriers by a sensor. However, the forces of wind barrier strips could be measured one by one. When testing one of the wind barrier strips, the strip is separated from cross beams, and other strips are still connected to cross beams. Each strip is tested in turn. A force sensor (see Fig. 4) is used in the force test whose range is 5 kg and accuracy is 0.5%. The sampling time and the sampling frequency are set to 50 s and 400 Hz, respectively. The sampling frequency is high enough to record the fluctuating signal of the aerodynamic forces acting on the wind barrier strips. The average of drag forces is used to calculate the aerodynamic coefficients.

The installation convenience of the wind barriers and measurement range and accuracy of the force sensor should be considered. Thus, the length of the wind barrier is divided into three sections: 1.7 m, 1.7 m and 1.0 m. The middle section is 1.0 m, which is set as the test section. The top and the bottom transition sections are 1.7 m and are used to avoid the influence of flow around the end of the test section (see Fig. 4).

Table 1 Parameters of wind barrier strips

Case	porosity of strips	Pore size (mm)	$H_f$ (mm)
Model-1	36.5%	6	300
Model-2	36.5%	16	300
Model-3	0%	0	219

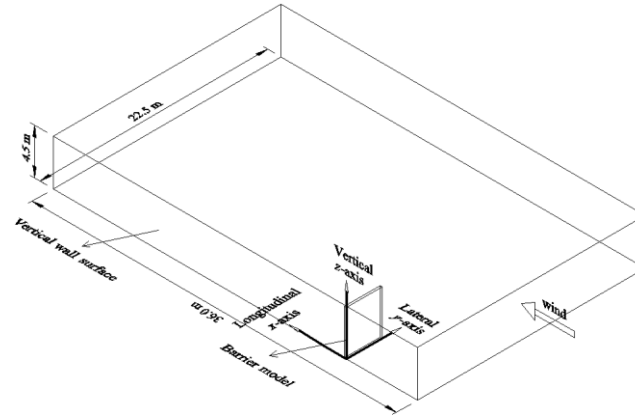


Fig. 3 Illustration of the wind barrier model and coordinate system used in the wind tunnel tests

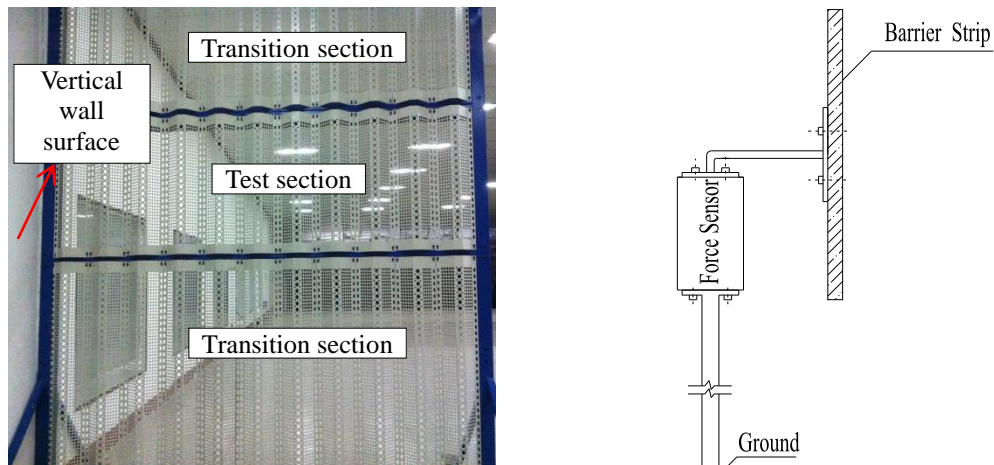


Fig. 4 Aerodynamic force test of wind barrier strips

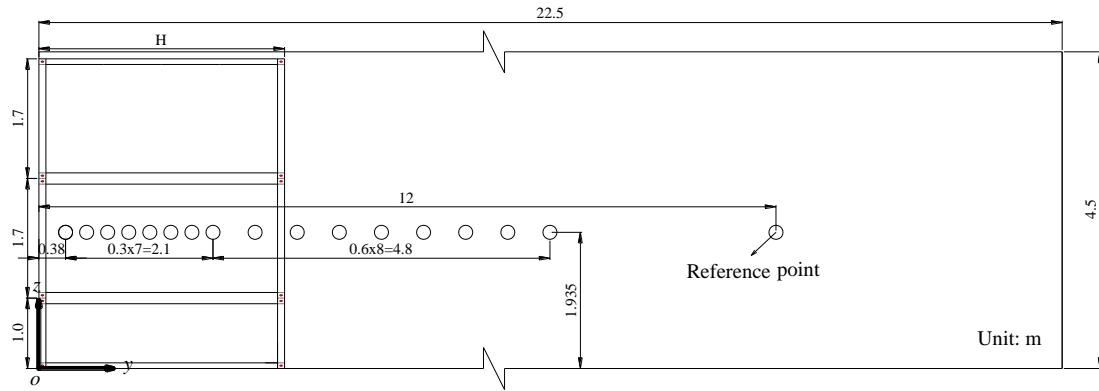
The drag coefficients of the wind barrier strips are given by Kwon, Kim *et al.* (2011)

$$C_{Hi} = \frac{F_{Hi}}{0.5\rho U_0^2 H_i L} \quad (1)$$

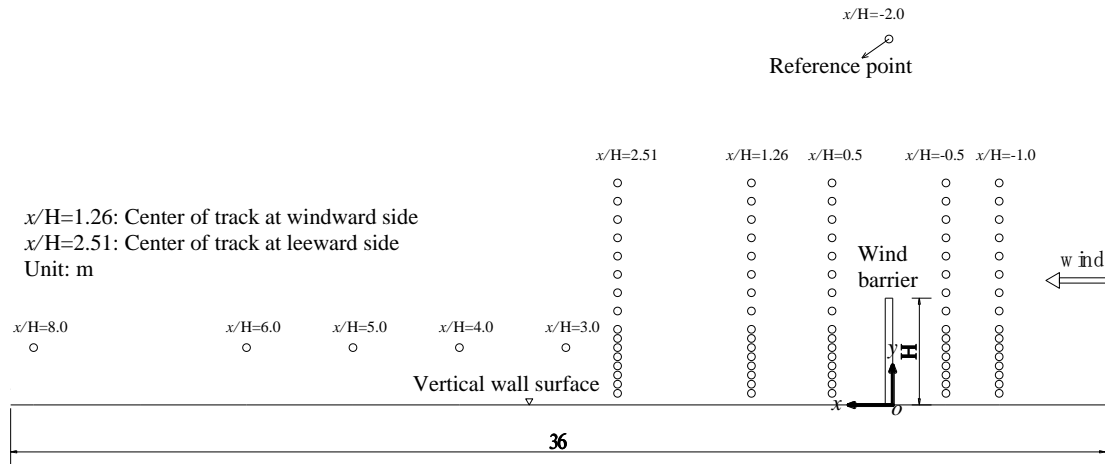
where  $F_{Hi}$  is the drag force of the wind barrier strips,  $H_i$  and  $L$  are the height and the length of the wind barrier strips of the test sections, respectively,  $U_0$  is the velocity of the approach flow, and  $\rho$  is the air density.

The drag coefficients of the entire wind barriers could be calculated by the following equation

$$C_{HZ} = \frac{\sum_{i=1} C_{Hi} \times H_i}{H} \quad (2)$$



(a) Side view from inlet



(b) Top view

Fig. 5 Locations of wind velocity measurements in the test section

Because that the interference of cross beams (see Fig. 2(a)) on the flow field could not be ignored. The test section changes places with the bottom transition section in a wind field test. Thus, the spacing of the middle section is set to 1.7 m. The mean wind velocities of the measured points located at different positions are collected using cobra probes. The sampling time and the sampling frequency are set to 60 s and 1250 Hz, respectively. Wind velocity measurements in this study are carried out at distances from the wind barrier of  $-1.0H$ ,  $-0.5H$ ,  $0.5H$ ,  $1.26H$ ,  $2.51H$ ,  $3.0H$ ,  $4.0H$ ,  $5.0H$ ,  $6.0H$  and  $8.0H$  along the  $x$ -axis of the test section (see Fig. 5(b)). It should be noted that distances from the wind barrier of  $1.26H$  ( $4.4$  m) and  $2.51H$  ( $8.8$  m) are the center of the track at the windward side and leeward side with reference to a railway bridge in practical engineering, respectively. The test points of wind velocities are set to sixteen different heights from  $0.38$  m to  $7.28$  m (see Fig. 5(a)). To ensure that the same initial wind speed is applied to all tests, a reference wind velocity is measured at the point  $x=0$ ,  $y=12$  m, and  $z=1.935$  m (see Fig. 5).

### 3. Scale effect of wind barriers

First, some studies have shown that streamlined structures (strips of model-3, for instance) are insensitive to the Reynolds number (Bearman 1969, Higuchi, Kim *et al.* 1989). According to a comparison of the flow fields and pressure coefficients between the full and model scales, it was concluded that a Reynolds number effect was present in the separated flows around bluff bodies (Hoxey, Reynolds *et al.* 1998). Based on the above observations, we could deduce that there would be some discrepancies of aerodynamic forces and wake characteristics downwind of wind barriers between full and model scales. This was proved by the work of Iversen (1989). Second, when scaling the wind barriers, we usually increased the pore size and reduced the pore number under the condition of holding the same ratio of porosity. This way might have an influence on the flow characteristics of wind barriers. Because the permeability has a significant effect on the bleed flow and is sensitive to the pore size (Raine and Stevenson 1977). Finally, the model-scale wind barriers could not easily simulate the local details accurately. All of the above indicated that a scale effect of wind barriers may exist in the scaled model wind tunnel test.

The drag coefficients of full-scale wind barriers are calculated with Eqs. (1) and (2) to compare with the scale model. Fig. 6 shows the drag coefficients  $C_{HZ}$  of full- and model-scale wind barriers, where the drag coefficients  $C_{HZ}$  of model-1, model-2 and model-3 are 0.893, 0.903 and 0.887, respectively. The model-scale wind barrier is a vertical perforated plate with a uniform circular hole, and the wind barrier is located at the ground roadbed (Xiang, Li *et al.* 2014). The drag force of the scale model is tested in wind tunnel XNJD-3 with a scale of 1/15 (Xiang 2013). Two porosities of the wind barrier of 30% and 40% are adopted. The heights of the wind barriers are 2.5 m, 2.95 m and 3.4 m. Although the blockage ratio, porosities, height and shape of model-scale barrier have some differences from the full-scale model, the comparison between the scale model results and the present study could reflect the scale influence indirectly (see Fig. 6). What we should pay attention to here is the height of the whole railway wind barriers is 3.3 m when calculating the drag coefficients, neglecting the columns.

In Fig. 6, the drag coefficients  $C_{HZ}$  of model-scale wind barriers are larger than those of full-scale wind barriers. The mechanism that causes this difference may be illustrated by considering the influence of the scale effect. The drag force on the wind barrier is related to the protective effect of the wind barrier (Miller, Rosenberg *et al.* 1975). Thus, testing on the flow characteristics of model-scale wind barriers may be unsafe.

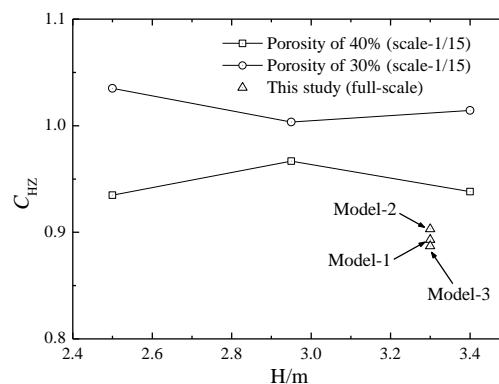


Fig. 6 Aerodynamic coefficients of entire wind barriers for model scale and full scale

## 4. Results and discussion

Flow fields behind barriers are complex by the presence of both the bleed flow that passes through the gaps in the barriers and the displaced flow that passes over the barriers (Dong, Luo *et al.* 2007). However, the airflows over wind barriers could be mainly regarded as two-dimensional. The airflow mainly moves in the  $x$ -direction (see Fig. 3), so the characteristics of flow fields in the longitudinal direction under different cases of wind barriers are mainly discussed in our study.

### 4.1 Effects of pore size

A study on the hole diameter effect of a porous fence is needed to understand the wake characteristics and to optimize the fence hole size (Kim and Lee 2001). However, the barrier models are very small, and the hole diameters are only 1.4 mm, 2.1 mm and 2.8 mm. Thus, the permeability of holes may not be presented accurately.

To investigate the effect of pore size on the flow field, the profiles of mean velocity and turbulence intensity for model-1 and model-2 are shown in Fig. 7. The wind velocity is normalized by the free-stream velocity  $U_0$  (11 m/s), and the height is normalized by the wind barrier height  $H$ .

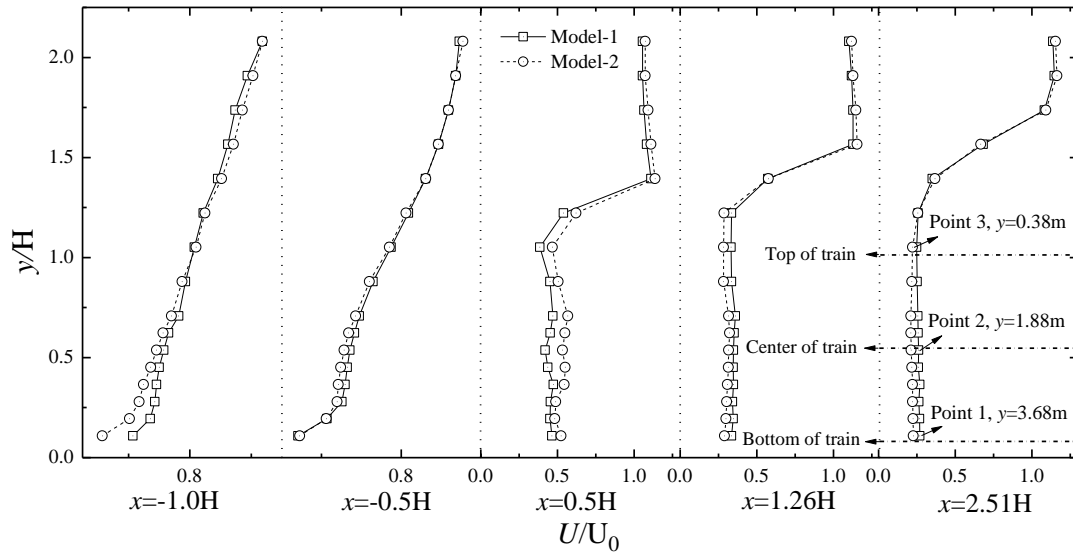
In Fig. 7(a), the mean velocity profiles upwind and downwind of the wind barriers have significant differences. Upwind, velocity increases with increasing height, and the velocities are less than the free-stream velocity. This is because of that a part of flow will reverse back to the opposite direction when the approach flow passing through wind barriers. Then a portion of approach flow is counteracted by the reverse flow, which causes the loss of the wind energy. So it leads to the lower of mean velocities. Downwind, an obvious shear layer is found. The height of the shear layer is in the region of  $1.0 < y/H < 1.5$ . The region below the height of the shear layer is regarded as the influence region of wind barriers (also called the protective region). In the protective region, the velocities are all less than the free-stream velocity, indicating that the wind barriers are effective at reducing wind velocity.

In Fig. 7(a), the mean velocity profiles of model-1 and model-2 upwind are in good agreement, revealing that the pore size has little effect on the upwind mean velocity field. Some differences in the mean velocity profiles between model-1 and model-2 are found at the location of  $x=0.5H$ . However, the differences gradually become slighter at distances from  $x=0.5H$  to  $2.51H$ . Velocities are lower for model-2 than for model-1 at  $x=1.26H$  and  $2.51H$ . This is mutually proved by the work of Kim and Lee (2001), in which it is concluded that the velocity reduction of a fence with a larger pore size of 2.8 mm is greater than that of a 2.1 mm fence. The mechanism could be explained as follows: the bleed-flow type jet passing through the fence holes causes a transition from laminar to turbulence and the jet coalescence effect seems to be occurred for the model-2.

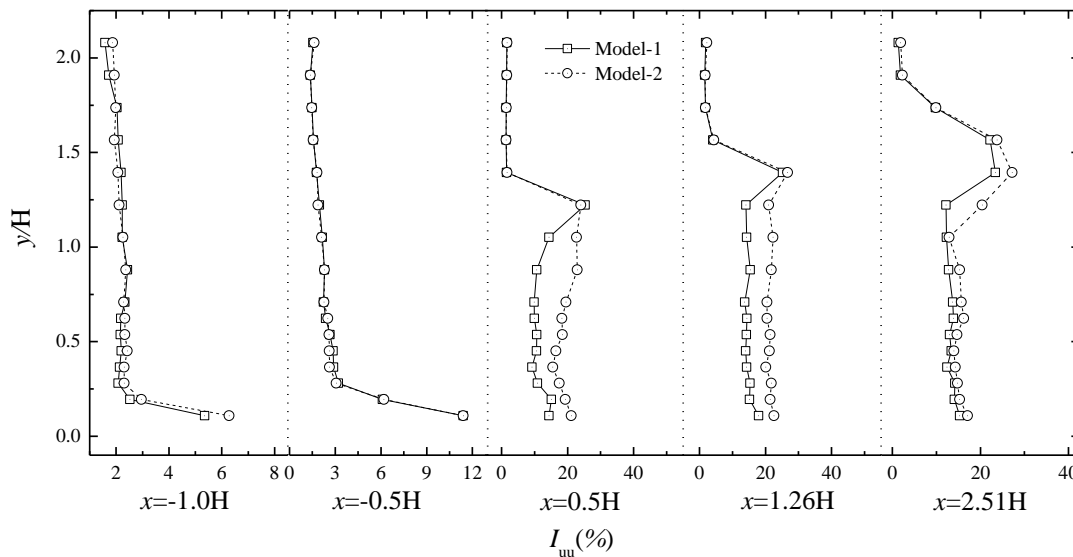
The turbulence field of airflow behind a barrier has significant impacts on the barrier's shelter efficiency (Dong, Luo *et al.* 2010). In Fig. 7(b), it is evident that the pore size has little effect on the upwind turbulence intensity profiles, whereas some effects exist downwind of the wind barrier. The turbulence intensity is lower for model-1 than for model-2. This is possible because bleed-flow passing through the holes influences each other and increases the turbulent intensity for model-2. As the flow goes downstream from  $0.5H$  to  $2.51H$ , the differences in the turbulence intensity profiles between model-1 and model-2 decrease gradually.

To further investigate the effect of pore size on the power spectra, Fig. 8 gives the power spectra of model-1 and model-2 at point 1, point 2 and point 3 (see Fig. 7(a)). In Fig. 8, point 1, point 2 and point 3 are near the bottom, center and top of train CRH2, respectively.

In Fig. 8(a), the power spectrum of model-1 at  $x=1.26H$  is slightly lower than that of model-2, especially for the low-frequency components. This suggests that smaller pore sizes generate lower power spectra. The effect of pore size on power spectrum will become slight with increasing  $x$  (see Fig. 8(b)).



(a)



(b)

Fig. 7 The flow fields of model-1 and model-2 (a) Mean velocity profiles and (b) Turbulence density profiles

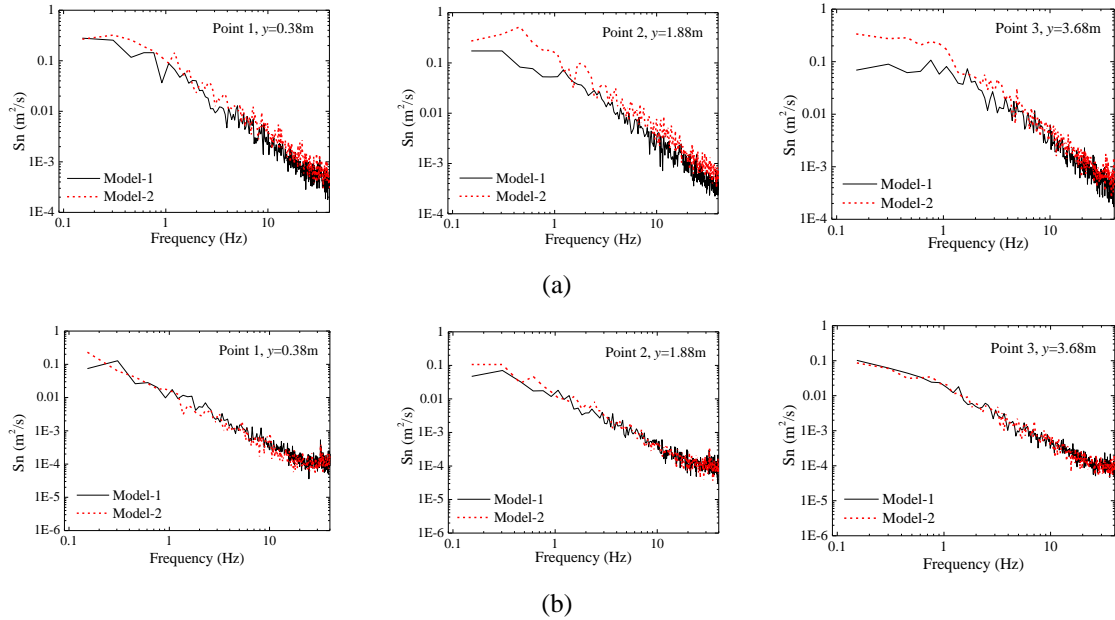


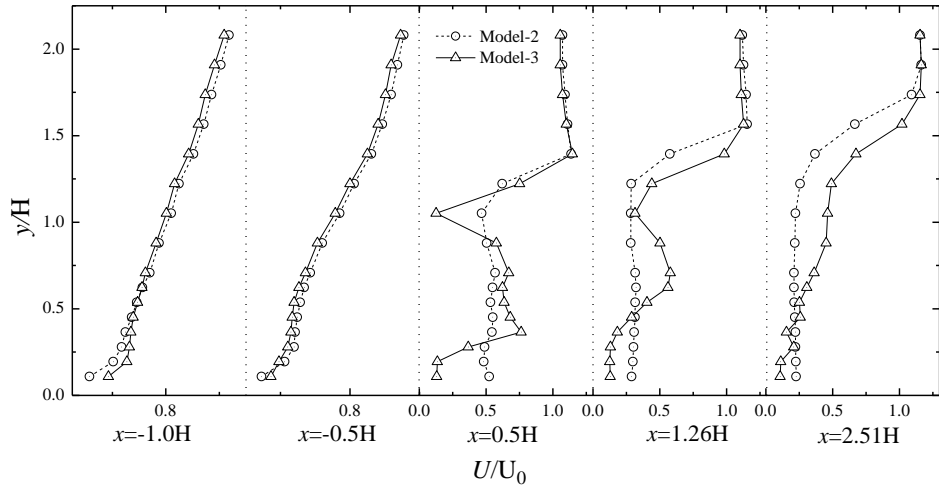
Fig. 8 The power spectra of model-1 and model-2 at three different heights (a)  $x = 1.26H$  and (b)  $x = 2.51H$

#### 4.2 Effects of different opening forms

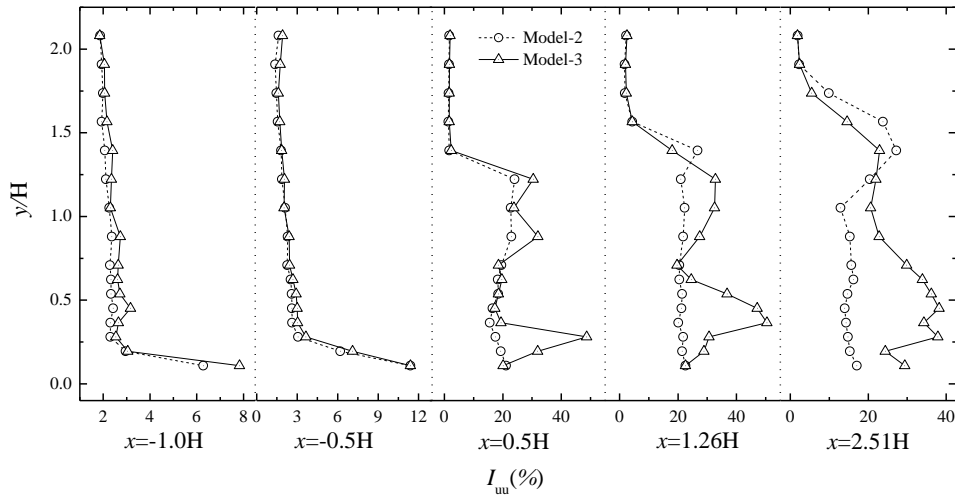
Different shapes of the open area of the wind barriers have some impacts on the protective (Yeh, Tsai *et al.* 2010). To investigate the effect of opening forms of wind barriers, Fig. 9 shows the mean velocity profiles and turbulence intensity profiles of model-2 and model-3. Fig. 10 gives the power spectra of three points in the presence of model-2 and model-3 at  $x=2.51H$ . In Figs. 9 and 10, the two different opening forms are porous (model-2) and bar-type (model-3).

In Fig. 9, the opening forms of wind barriers have a slight impact on the upwind mean velocity field and turbulence intensity. However, the opening forms of wind barriers have a significant impact on the downwind mean velocity and turbulence intensity below the height of the shear layer. In Fig. 9(a), the mean velocity profile of model-3 at  $x=0.5H$  to  $1.26H$  is very non-uniform; as a result, velocities on the backs of the strips are small, whereas the velocities located in the gaps between two adjacent strips are large. This also leads to the non-uniform distribution of turbulence intensity for model-3 (see Fig. 9(b)). The porous wind barrier may give better protection than the bar-type wind barrier from the aspect of the mean velocity field at  $x=1.26H$  and  $2.51H$ .

In Fig. 10, the power spectra of model-3 at point 1 shows a significant reduction in the low frequency range (0–7 Hz), and the power spectrum of model-3 at frequencies above 7 Hz is larger than that of model-2. Regarding point 2 and point 3, in the entire frequency range, model-2 shows a lower power spectrum than model-3. This further suggests that model-2 is more beneficial in reducing the vibration of vehicles.



(a)



(b)

Fig. 9 The flow fields of model-2 and model-3 (a) Mean velocity profiles and (b) Turbulence density profiles

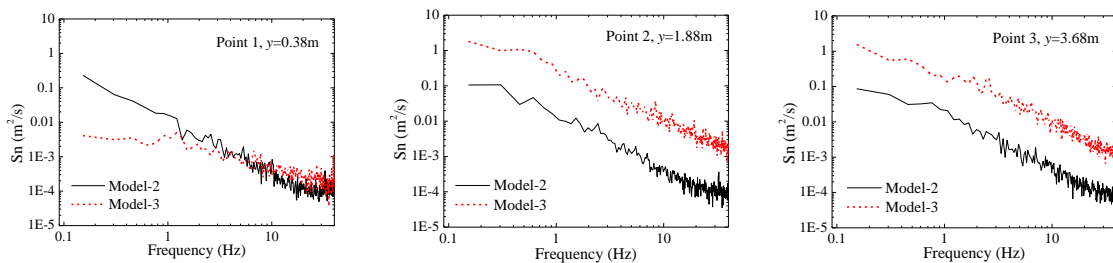


Fig. 10 The power spectra of model-2 and model-3 at three different heights when  $x = 2.51H$

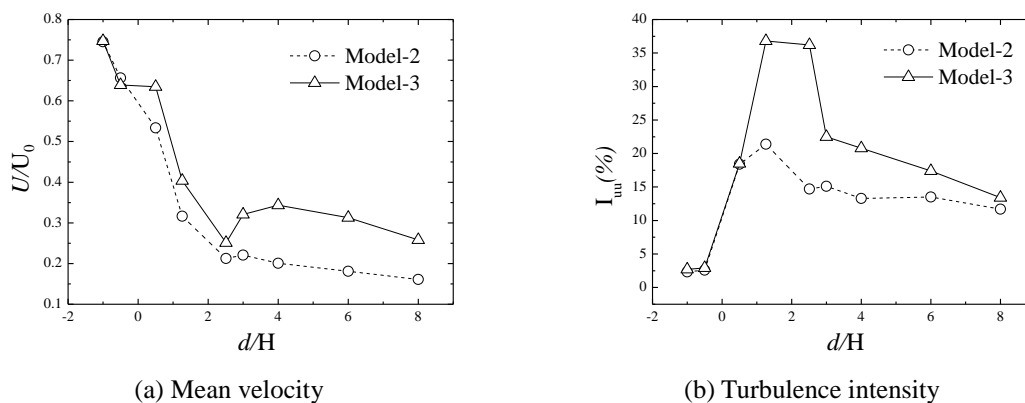


Fig. 11 Mean velocity and turbulence intensity profiles along  $x$ -axis at  $y=1.88$  m

#### 4.3 The effective shelter distance of the wind barrier

Assessment of the shelter effect of wind barriers should consider not only the absolute reduction in wind velocity but also the area or distance that is sheltered (Dong, Qian *et al.* 2006). Although the distance between the wind barrier and the track on the bridge (or high embankment) is fixed, it is meaningful to explore the protected distances of the railway wind barrier setting on the ground roadbed. Fig. 11 shows the mean velocity and turbulence intensity profiles of model-2 and model-3 along the  $x$ -axis at  $y=1.88$  m. The measuring height is close to the height of the centerline of the train body for CRH2 (1.95 m above the orbit) and the center of the wind barrier.

In Fig. 11(a), there is an obvious difference between model-2 and model-3. Downwind from  $0.5H$  to  $2.51H$ , velocities of model-2 and model-3 decrease with increasing  $x$ , and the velocities are much lower for model-2 than for model-3. At  $x=3.0H$ , the mean velocity increases obviously for model-3 yet slightly for model-2. At distances from  $4.0H$  to  $8.0H$ , the mean velocities decrease gradually, and the difference in the velocities between the two wind barriers is relatively large. Based on the above comparisons, we can conclude that model-2 provides better shelter than model-3 downwind of the wind barrier. Furthermore, the mean velocity significantly decreases near the two wind barriers. For example, the values of  $U/U_0$  at  $x=8.0H$  for model-2 and model-3 are 0.161 and 0.258, respectively, indicating that the location of  $8H$  is still in the protection zone of wind barriers in the two cases of model-2 and model-3.

In Fig. 11(b), it is obvious that the turbulence intensity in the case of model-2 is more uniform than in the case of model-3. At distances from  $-1.0H$  to  $8.0H$ , the turbulence intensity of two wind barriers first increases and then decreases. At the distance of  $8H$ , the turbulence intensity of the two cases is almost the same (tending to be 10%). Moreover, the difference in the turbulence intensity between model-2 and model-3 first increases and then decreases.

## 5. Conclusions

In wind tunnel tests, the flow fields of full-scale railway wind barriers are collected with respect to three wind barriers, and then the results are analyzed and discussed. Some conclusions

can be drawn on the basis of the foregoing analysis.

- It is evident that a scale effect is present in the separated flows around wind barriers, and testing on the characteristics of model-scale wind barriers may be unsafe. More detailed work is required to produce generalized correction terms for extrapolation from model-scale to full-scale values, as is required to obtain reliable design information.
- The pore size and opening forms of full-scale wind barriers have a slight influence on the characteristics of flow fields upwind, but they have a significant influence on the downwind flow fields within a certain range. The smaller pore size generates a lower turbulence density and value of the power spectrum near the wind barrier, and the porous wind barriers clearly provide better shelter than the bar-type wind barriers.
- At distances from  $-1.0H$  to  $8H$ , mean wind velocities decrease generally. The turbulence intensity first increases and then decreases. It is concluded that the distance of  $8H$  downwind of the wind barrier is still in the effective protection region of wind barriers.

## Acknowledgments

The research described in this paper was supported by the National Natural Science Foundation of China (Grant No. NNSF-U1334201; 51408503; 51525804), the National Basic Research Program of China (“973” Project) (Grant No. 2013CB036206), and the Sichuan Province Youth Science and Technology Innovation Team (Grant No. 2015TD0004).

## References

- Bearman, P.W. (1969), “On vortex shedding from a circular cylinder in the critical Reynolds number regime”, *J. Fluid Mech.*, **37**(3), 577-585.
- Bitog, J.P., Lee, I.B., Shin, M.H., Hong, S.W., Hwang, H.S., Seo, I.H., Yoo, J.I., Kwon, K.S., Kim, Y.H. and Han, J.W. (2009), “Numerical simulation of an array of fences in Saemangeum reclaimed land”, *Atmos Environ.*, **43**(30), 4612-4621.
- Bofah, K.K. and Al-Hinai, K.G. (1986), “Field tests of porous fences in the regime of sand-laden wind”, *J. Wind Eng. Ind. Aerod.*, **23**, 309-319.
- Boldes, U., Colman, J. and Di Leo, J.M. (2001), “Field study of the flow behind single and double row herbaceous windbreaks”, *J. Wind Eng. Ind. Aerod.*, **89**(7), 665-687.
- Chen, N., Li, Y.L., Wang, B., Su, Y. and Xiang, H.Y. (2015), “Effects of wind barrier on the safety of vehicles driven on bridges”, *J. Wind Eng. Ind. Aerod.*, **143**, 113-127.
- Chu, C.R., Chang, C.Y., Huang, C.J., Wu, T.R., Wang, C.Y. and Liu, M.Y. (2013), “Windbreak protection for road vehicles against crosswind”, *J. Wind Eng. Ind. Aerod.*, **116**, 61-69.
- Coleman, S.A. and Baker, C.J. (1992), “The reduction of accident risk for high sided road vehicles in cross winds”, *J. Wind Eng. Ind. Aerod.*, **44**(1-3), 2685-2695.
- Dong, Z.B., Luo, W.Y., Qian, G.Q., Lu, P. and Wang, H.T. (2010), “A wind tunnel simulation of the turbulence fields behind upright porous wind fences”, *J. Arid Environ.*, **74**(2), 193-207.
- Dong, Z.B., Luo, W.Y., Qian, G.Q. and Wang, H.T. (2007), “A wind tunnel simulation of the mean velocity fields behind upright porous fences”, *Agr. Forest Meteorol.*, **146**(1), 82-93.
- Dong, Z.B., Qian, G.Q., Luo, W.Y. and Wang, H.T. (2006), “Threshold velocity for wind erosion: the effects of porous fences”, *Environ. Geology.*, **51**(3), 471-475.
- Guo, W.W., Wang, Y.J., Xia, H. and Lu, S. (2014), “Wind tunnel test on aerodynamic effect of wind barriers on train-bridge system”, *Sci. China Tech. Sci.*, **58**(2), 219-225.

- Higuchi, H., Kim, H.J. and Farell, C. (1989), “Flow separation and reattachment around a circular cylinder at critical Reynolds numbers” *J. Fluid Mech.*, **200** 149-171.
- Hoxey, R.P., Reynolds, A.M., Richardson, G.M., Robertson, A.P. and Short, J.L. (1998), “Observations of Reynolds number sensitivity in the separated flow region on a bluff body”, *J. Wind Eng. Ind. Aerod.*, **73**(3), 231-249.
- Iversen, J.D. (1981), “Comparison of wind-tunnel model and full-scale snow fence drifts”, *J. Wind Eng. Ind. Aerod.*, **8**(3), 231-249.
- Kim, H.B. and Lee, S.J. (2001), “Hole diameter effect on flow characteristics of wake behind porous fences having the same porosity”, *Fluid Dyn. Res.*, **28**, 449-464
- Kozmar, H., Procino, L., Borsani, A. and Bartoli, G. (2012), “Sheltering efficiency of wind barriers on bridges”, *J. Wind Eng. Ind. Aerod.*, **107-108** 274-284.
- Kwon, S., Kim, D.H., Lee, S.H. and Song, H.S. (2011), “Design criteria of wind barriers for traffic -Part 1: wind barrier performance”, *Wind Struct.*, **14**(1), 55-70.
- Lee, S. and Kim, H. (1999), “Laboratory measurements of velocity and turbulence field behind porous fences”, *J. Wind Eng. Ind. Aerod.*, **80**(3), 311-326.
- Miller, D.R., Rosenberg, N.J. and Bagley, W.T. (1975), “Wind reduction by a highly permeable tree shelterbelt”, *Agricultural Meteorol.*, **14**, 321-333.
- Raine, J.K. and Stevenson, D.C. (1977), “Wind protection by model fences in a simulated atmospheric boundary layer”, *J. Wind Eng. Ind. Aerod.*, **2**(2), 159-180.
- Richardson, G. (1995), “Full-scale measurements of the effect of a porous windbreak on wind spectra”, *J. Wind Eng. Ind. Aerod.*, **54-55**, 611-619.
- Schwartz, R.C., Fryrear, D.W., Harris, B.L., Bilbro, J.D. and Juo, A. (1995), “Mean flow and shear stress distributions as influenced by vegetative windbreak structure”, *Agr. Forest Meteorol.*, **75**(1), 1-22.
- Telenta, M., Batista, M., Biancolini, M.E., Prebil, I. and Duhovnik, J. (2015), “Parametric numerical study of wind barrier shelter”, *Wind Struct.*, **20**(1), 75-93.
- Telenta, M., Duhovnik, J., Kosel, F. and Šajn, V. (2014), “Numerical and experimental study of the flow through a geometrically accurate porous wind barrier model”, *J. Wind Eng. Ind. Aerod.*, **124** 99-108.
- Wang, D.L., Wang, B.J. and Chen, A.R. (2013), “Vehicle-induced aerodynamic loads on highway sound barriers part1: field experiment”, *Wind Struct.*, **17**(4), 435-449.
- Wu, X.X., Zou, X.Y., Zhang, C.L., Wang, R.D., Zhao, J. and Zhang, J. (2013), “The effect of wind barriers on airflow in a wind tunnel”, *J. Arid Environ.*, **97** 73-83.
- Xiang, H.Y. (2013), Protection effect of wind barrier on high speed railway and its wind loads, PhD. Chengdu: Southwest Jiaotong University, (in Chinese).
- Xiang, H.Y., Li, Y.L., Chen, B. and Liao, H.L. (2014), “Protection effect of railway wind barrier on running safety of trainu cross winds”, *Adv. Struct. Eng.*, **17**(8), 1177-1188.
- Xiang, H.Y., Li, Y.L. and Wang, B. (2015a), “Aerodynamic interaction between static vehicles and wind barriers on railway bridges exposed to crosswinds”, *Wind Struct.*, **20**(2), 237-247.
- Xiang, H.Y., Li, Y.L., Wang, B. and Liao, H.L. (2015b), “Numerical simulation of the protective effect of railway wind barriers under crosswinds”, *Int. J. Rail Transportation.*, **3**(3), 151-163.
- Yeh, C.P., Tsai, C.H. and Yang, R.J. (2010), “An investigation into the sheltering performance of porous windbreaks under various wind directions”, *J. Wind Eng. Ind. Aerod.*, **98**(10-11), 520-532.